Path-Dependent Rollover Prevention for Critical Truck Maneuvers

K. Lundahl, C.F. Lee, E. Frisk & L. Nielsen
Division of Vehicular Systems, Department of Electrical Engineering, Linköping University, Sweden

ABSTRACT: Predicting rollover is usually performed using rollover indices, where rollover is anticipated when the indices reach certain threshold values. If knowledge about the vehicle driving path is available, rollover can be detected and prevented earlier. In this work, the rollover-prediction and rollover-prevention abilities for simple vehicle models are evaluated and compared against a high-fidelity vehicle model. The analysis is performed by using the models in critical and rollover-prone maneuvers, generated with optimal control methods. The main conclusion is that a simple point-mass model would be sufficient in a velocity based rollover-prevention controller.

1 INTRODUCTION

The push towards autonomously driven vehicles, with ambition to operate on public roads and within enclosed sites, opens up a wide area of research questions that need to be addressed. For this particular purpose, the iQMatic project was initiated in 2013 as a joint collaboration between Scania, Saab, Autoliv, Linköping University and the Royal Institute of Technology. The aim is to develop fully autonomous heavy vehicles, which implies problems regarding vehicle navigation, obstacle avoidance, and decision making, to name a few, has to be solved. In this paper, the isolated problem of vehicle rollover is investigated.

Predicting rollover is usually performed using rollover indices, continuously calculated on-board from sensor data, where rollover is anticipated when the indices reach certain threshold values (Winkler et al., 2000; Liu et al., 1997). If knowledge about the vehicle driving path is available, the risk of rollover can be detected earlier, and avoidance action can be initiated with greater chance of preventing the accident. For example, if a vehicle overspeeds into a road curve, it might be to late to take action when the rollover indices indicate a risk of rollover. However, this could have been anticipated if information about the road curvature was available, and may be avoided by reducing the vehicle speed in advance.

Motivated by the above, we investigate the use of a path-dependent approach to rollover prevention. Since the application is aimed towards on-board control systems, vehicle models of low complexity are preferred due to the often limited computational power. However, with reduced modeling complexity there is always a risk of losing model precision. Therefore, a comparison is presented for two low-complexity models versus a high-fidelity vehicle dynamics model, with respect to their ability to foresee vehicle rollover. To support this analysis an optimal-control based approach is presented, using maximum-speed and minimum-time problem formulations to generate rollover-critical scenarios.

2 METHOD

The aim is to evaluate the potential simple models have with respect to rollover prediction, when compared to a complex and more versatile vehicle model. The models of interest are a point-mass model, an inverted pendulum model, and a double-track model. The latter will here be used as the reference model against which the former two are evaluate.

The analysis is performed by formulating optimal control problems in which the models are used. In these problems, the vehicle models are subject to follow a predefined path constructed by clothoids. The first out of two problem formulations is a maximum-speed problem, where

the vehicle is constrained to constant velocity. The obtained result declare the maximum speed the vehicle can drive through the given road path. For example, if an on-board controller detects the current vehicle speed is above this threshold, the control system has to take action to prevent rollover. The second problem formulation address this situation. A minimum-time problem formulation is used, implying the vehicle will maintain the highest possible speed, for as long as possible. When only braking is allowed, this will return an optimal solution describing the very last moment action needs to be taken to avoid rollover.

3 MODELING

The vehicle dynamics are represented by three different models, here referred to as the point-mass model, the pendulum model, and the double-track model. These models are here presented in detail, followed by a description of the vehicle path formulation. The vehicle and tire parameters used for these models are listed in Table 1 and 2.

3.1 *Double-Track Model*

The double-track model (sometimes referred to as a two-track model) is depicted in Figure 1. This model consists of a single inertia body representing the vehicle's total mass m and moment of inertia I_{xx}, I_{yy}, and I_{zz}. The body is suspended as an inverted pendulum, with the freedom to revolve about the x-axis around the roll center (at height h_{rc}), and about the y-axis around the pitch center (located in the ground plane, right beneath the center of gravity). These degrees of freedoms represents the roll and pitch motions respectively. The body position $\mathbf{r}_b$ with respect to, and resolved in, the vehicle frame (represented by x, y, z in Figure 1) can therefore be described as

$$\mathbf{r}_b = R_\theta \left(R_\phi \begin{bmatrix} 0 \\ 0 \\ h_{cg} - h_{rc} \end{bmatrix} + \begin{bmatrix} 0 \\ 0 \\ h_{rc} \end{bmatrix} \right) \tag{1}$$

where R_ϕ and R_θ are roll and pitch rotation matrices according to

$$R_\phi = \begin{bmatrix} 1 & 0 & 0 \\ 0 & \cos\phi & -\sin\phi \\ 0 & \sin\phi & \cos\phi \end{bmatrix}, \quad R_\theta = \begin{bmatrix} \cos\theta & 0 & \sin\theta \\ 0 & 1 & 0 \\ -\sin\theta & 0 & \cos\theta \end{bmatrix}. \tag{2}$$

The motion dynamics are derived using Lagrange's equations, with the generalized motion variables longitudinal velocity v_x, lateral velocity v_y, roll angle ϕ, pitch angle θ, and yaw angle ψ. The motion dynamics for the vehicle body can thus be expressed as

$$\frac{\mathrm{d}}{\mathrm{dt}}\frac{\partial \mathcal{L}}{\partial v_x} - \dot{\psi}\frac{\partial \mathcal{L}}{\partial v_y} = (F_{x,1} + F_{x,2})\cos\delta - (F_{y,1} + F_{y,2})\sin\delta + F_{x,3} + F_{x,4} \tag{3}$$

$$\frac{\mathrm{d}}{\mathrm{dt}}\frac{\partial \mathcal{L}}{\partial v_y} + \dot{\psi}\frac{\partial \mathcal{L}}{\partial v_x} = (F_{y,1} + F_{y,2})\cos\delta + (F_{x,1} + F_{x,2})\sin\delta + F_{y,3} + F_{y,4} \tag{4}$$

$$\frac{\mathrm{d}}{\mathrm{dt}}\frac{\partial \mathcal{L}}{\partial \dot{\phi}} - \frac{\partial \mathcal{L}}{\partial \phi} + \frac{\partial \mathcal{F}}{\partial \phi} = 0 \tag{5}$$

$$\frac{\mathrm{d}}{\mathrm{dt}}\frac{\partial \mathcal{L}}{\partial \dot{\theta}} - \frac{\partial \mathcal{L}}{\partial \theta} + \frac{\partial \mathcal{F}}{\partial \theta} = 0 \tag{6}$$

$$\begin{aligned}\frac{\mathrm{d}}{\mathrm{dt}}\frac{\partial \mathcal{L}}{\partial \dot{\psi}} - \frac{\partial \mathcal{L}}{\partial \psi} = {} & l_f((F_{y,1} + F_{y,2})\cos\delta + (F_{x,1} + F_{x,2})\sin\delta) - l_r(F_{y,3} + F_{y,4}) + \\ & + w((-F_{x,1} + F_{x,2})\cos\delta + (F_{y,1} - F_{y,2})\sin\delta + F_{x,3} + F_{x,4})\end{aligned} \tag{7}$$

where the right-hand side are the generalized forces, composed by the longitudinal and lateral tire forces in Equation 3, 4, and 7. In Equation 5 and 6 the generalized forces are zero, since road

profile variations are neglected. The Lagrangian $\mathcal{L}$ is formed by the kinetic $\mathcal{T}$ and potential energy $\mathcal{V}$, according to

$$\mathcal{L} = \mathcal{T} - \mathcal{V} \tag{8}$$

$$\mathcal{T} = \frac{1}{2} m \mathbf{v}_b^T \mathbf{v}_b + \frac{1}{2} \boldsymbol{\omega}_b^T \mathbf{I} \boldsymbol{\omega}_b \tag{9}$$

$$\mathcal{V} = \frac{1}{2}(K_{\phi,f} + K_{\phi,r})\phi^2 + \frac{1}{2} K_\theta \theta^2 + mg(h_{rc}\cos\theta + (h_{cg} - h_{rc})\cos\phi) \tag{10}$$

where $\mathbf{v}_b$ and $\boldsymbol{\omega}_b$ are the translational and rotational velocities of the vehicle body, resolved in the vehicle frame, and $\mathbf{I} = \mathrm{diag}(I_{xx}, I_{yy}, I_{zz})$ the inertia matrix. The vehicle's suspension system is modeled as a rotational spring-and-damper system, with front and rear roll stiffness $K_{\phi,f}, K_{\phi,r}$, and pitch stiffness K_θ. Similarly, the suspension damping is represented by rotational dampers, denoted $D_{\phi,f}, D_{\phi,r}, D_\theta$, embedded in the motion equations by the dissipation function $\mathcal{F}$ as

$$\mathcal{F} = \frac{1}{2}(D_{\phi,f} + D_{\phi,r})\dot{\phi}^2 + \frac{1}{2} D_\theta \dot{\theta}^2. \tag{11}$$

The longitudinal and lateral load transfer between the wheels are represented by

$$(F_{z,1} + F_{z,2})l_f - (F_{z,3} + F_{z,4})l_r = K_\theta \theta + D_\theta \dot{\theta}\,, \quad \sum_{i=1}^{4} F_{z,i} = mg \tag{12}$$

$$-w(F_{z,1} - F_{z,2}) = (F_{y,1} + F_{y,2})h_{rc} + K_{\phi,f}\phi + D_{\phi,f}\dot{\phi} \tag{13}$$

$$-w(F_{z,3} - F_{z,4}) = (F_{y,3} + F_{y,4})h_{rc} + K_{\phi,r}\phi + D_{\phi,r}\dot{\phi} \tag{14}$$

where F_z are the vertical tire forces and the indices $1, 2, 3, 4$ denote the respective wheel.

The slip angle α and slip ratio κ are defined as in (Pacejka, 2006),

$$\dot{\alpha}_i \frac{\sigma}{v_{x,i}} + \alpha_i = -\arctan\left(\frac{v_{y,i}}{v_{x,i}}\right), \qquad \kappa_i = \frac{R_w\omega_i - v_{x,i}}{v_{x,i}} \tag{15}$$

where ω_i is the wheel angular velocity, σ the relaxation length, and $v_{x,i}, v_{y,i}$ are the longitudinal and lateral velocities resolved in the wheel specific coordinate systems. The notation i represents the wheel number, where $i \in \{1, 2, 3, 4\}$. This is also used in the remaining equations for the double-track model.

The wheel dynamics are given by

$$T_i - I_w\dot{\omega}_i - F_{x,i}R_w = 0 \tag{16}$$

where T_i is the wheel driving/braking torque, I_w the wheel inertia, and R_w the wheel radius.

The longitudinal and lateral tire forces are computed according to (Pacejka, 2006). First, the nominal tire forces $F_{x0,i}, F_{y0,i}$ are calculated for pure slip. Subsequently, the final tire forces $F_{x,i}, F_{y,i}$ are determined, taking combined slip in consideration by using the weighting functions $G_{x\alpha,i}, G_{y\kappa,i}$. The complete tire force equations follows from

$$F_{x0,i} = \mu_{x,i} F_{z,i} \sin(C_{x,i} \arctan(B_{x,i}\kappa_i - E_{x,i}(B_{x,i}\kappa_i - \arctan B_{x,i}\kappa_i))) \tag{17}$$

$$F_{y0,i} = \mu_{y,i} F_{z,i} \sin(C_{y,i} \arctan(B_{y,i}\alpha_i - E_{y,i}(B_{y,i}\alpha_i - \arctan B_{y,i}\alpha_i))) \tag{18}$$

$$G_{x\alpha,i} = \cos(C_{x\alpha,i} \arctan(B_{x1,i} \cos(\arctan(B_{x2,i}\kappa_i))\alpha_i)) \tag{19}$$

$$F_{x,i} = F_{x0,i} G_{x\alpha,i} \tag{20}$$

$$G_{y\kappa,i} = \cos(C_{y\kappa,i} \arctan(B_{y1,i} \cos(\arctan(B_{y2,i}\alpha_i))\kappa_i)) \tag{21}$$

$$F_{y,i} = F_{y0,i} G_{y\kappa,i}. \tag{22}$$

3.2 *Point-Mass Model*

The second model is a planar model, consisting of a single inertia body with mass m, velocity v, and yaw direction ψ. The acceleration a_x and yaw acceleration u_ψ are considered as inputs,

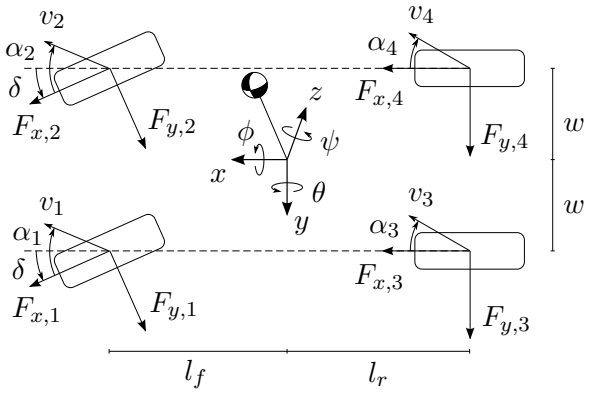

Figure 1. Double-track model.

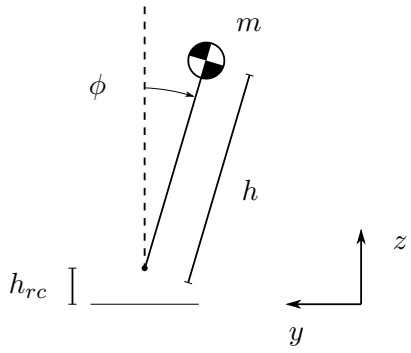

Figure 2. Pendulum model.

Table 1. Vehicle model parameters.

Notation	Value	Unit
l_f	2.45	m
l_r	2.55	m
w	1.05	m
m	16 200	kg
I_{xx}	24 500	kgm^2
I_{yy}	152 800	kgm^2
I_{zz}	207 900	kgm^2
R_w	0.5	m
I_w	100	kgm^2
σ	0.5	m
g	9.807	m/s^2
h_{cg}	1.66	m
h_{rc}	0.50	m
$K_{\phi,f}, K_{\phi,r}$	706	kNm/rad
$D_{\phi,f}, D_{\phi,r}$	103	kNms/rad
K_θ	2 450	kNm/rad
D_θ	1 170	kNms/rad

Table 2. Tire model parameters.

Notation	Value
μ_x	0.85
B_x	11.7
C_x	1.69
E_x	0.377
μ_y	0.75
B_y	8.86
C_y	1.19
E_y	-1.21
B_{x1}	12.4
B_{x2}	-10.8
$C_{x\alpha}$	1.09
B_{y1}	6.46
B_{y2}	4.20
$C_{y\kappa}$	1.08

forming the simple equations of motion

$$\dot{v} = a_x \tag{23}$$

$$\ddot{\psi} = u_\psi. \tag{24}$$

The lateral load transfer for the rear axle is derived by assuming stationary roll dynamics and taking the front and rear roll stiffness into consideration, resulting in

$$\Delta \bar{F}_{z,r} = -\frac{1}{F_{z,r}} \frac{m a_y}{w} \left(h_{cg} \frac{l_f}{l} + (h_{cg} - h_{rc}) \frac{K_{\phi,r}}{K_{\phi,f} + K_{\phi,r} - mg(h_{cg} - h_{rc})} \right) \tag{25}$$

where the wheel base l is given by $l = l_f + l_r$, and the lateral acceleration by $a_y = v\dot{\psi}$. The longitudinal load transfer will change the load on the rear axle during braking and acceleration. The vertical load on the rear axle $F_{z,r}$, is therefore computed according to

$$F_{z,r} = mg \frac{l_f}{l} + m a_x \frac{h_{cg}}{l}. \tag{26}$$

3.3 *Pendulum Model*

The pendulum model is similar to the point-mass model, however, with added roll dynamics according to

$$(I_{xx} + m(h_{cg} - h_{rc})^2)\ddot{\phi} + (D_{\phi,f} + D_{\phi,r})\dot{\phi} + (K_{\phi,f} + K_{\phi,r})\phi = \\ = ma_y(h_{cg} - h_{rc})\cos\phi + mg(h_{cg} - h_{rc})\sin\phi \quad (27)$$

The lateral load transfer for the rear axle is determined similarly to Equation 25, but with added roll dynamics according to

$$\Delta\bar{F}_{z,r} = -\frac{1}{F_{z,r}}\frac{ma_y}{w}\left(h_{cg}\frac{l_f}{l} + (h_{cg} - h_{rc})\frac{K_{\phi,r}}{K_{\phi,f} + K_{\phi,r} - mg(h_{cg} - h_{rc})}\right) \quad (28)$$

where $F_{z,r}$ is given by Equation 26.

3.4 *Driving Path*

The predetermined driving path is described by a curvilinear abscissa s (Cossalter et al., 1999; Limebeer and Rao, 2015). The vehicle position is represented by s, describing the traveled distance along the path, and the perpendicular deviation e from the path. The path dynamics are formulated according to

$$\dot{s} = \frac{v\cos(\psi - \psi_s)}{1 - eC} \quad (29)$$

$$\dot{\psi}_s = \dot{s}C \quad (30)$$

$$\dot{e} = v\sin(\psi - \psi_s) \quad (31)$$

where ψ_s is the tangential direction of the path, ψ the vehicle yaw angle, and v the absolute vehicle velocity. The path curvature (i.e., inverse of curve radius) is described by the s dependent function C. The path is divided into several segments, where s_k defines the start of segment k, and C_k represent the curvature over this segment. The path segments are then stitched together using sigmoid functions h_k to a single continuous function C, according to

$$h_k = \frac{1}{1 + e^{-(s - s_k)}} - \frac{1}{1 + e^{-(s - s_{k+1})}} \quad (32)$$

$$C = \sum_{k=1}^{N} h_k C_k \quad (33)$$

The total number of segments N varies depending on the path of interest.

4 OPTIMAL CONTROL PROBLEM

The vehicle and path models described in Section 3 are formulated as ordinary differential equation systems according to $\dot{x}(t) = f(x(t), u(t))$, with x representing the model states and u the control variables. The control variables are $u = [\dot{\delta}, T_1, T_2, T_3, T_4]^T$ for the double-track model, and $u = [u_\psi, a_x]^T$ for the point-mass model and the pendulum model. The optimal control problem to solve is formulated as

$$\begin{aligned} \text{minimize} \quad & J \\ \text{subject to} \quad & \dot{x}(t) = f(x(t), u(t)), \\ & g(x(t), u(t)) \leq 0, \\ & x(0) = x_0, \qquad x(t_f) = x_{t_f}, \qquad t \in [0, t_f] \end{aligned} \quad (34)$$

where J is the objective function and t_f the terminal time. The continuous constraints are described by $g(x, u)$, while the initial and terminal constraints are formulated with x_0 and x_{t_f}.

Wheel lift is prevented with the constraints $F_{z,i} \geq 0,\ i \in \{1,2,3,4\}$ for the double-track model, and $|\Delta F_{z,r}| \leq 1$ for the remaining two models.

Two different cases are considered. In the first, the vehicle velocity is kept constant by introducing the constraint $\dot{v} = 0$, and the objective is to maximize the initial velocity $v(0) = v_0$. The cost function is formulated according to

$$J_1 = -v_0 + \eta \int_0^{t_f} u^T Q u \, \mathrm{dt} \tag{35}$$

where u is added to prevent unnecessary and oscillating control actuation. However, the contribution is kept comparatively small with a weight factor of $\eta = 10^{-3}$. The constant matrix Q is normalizing the control inputs to equivalent measures for the different models.

The second case of study is formulated as a time-optimal problem, with a fixed initial velocity. The constraints $a_x \leq 0$ for the point-mass model and $T_i \leq 0,\ i \in \{1,2,3,4\}$ for the double track model are introduced. This implies the vehicle velocity can vary, but only braking is allowed (i.e., the vehicle can not accelerate). Accordingly, the objective function is

$$J_2 = t_f + \eta \int_0^{t_f} u^T Q u \, \mathrm{dt} \, . \tag{36}$$

The continuous optimal-control problems formulated above are solved with numerical methods, using the software platform CasADi (Andersson, 2013). First, the problem is discretized over the time horizon into 200 elements using Radau collocation. In each element, the state dynamics are approximated with third order polynomials using three collocation points, while the control variables are constant over each discretization interval. The resulting discrete-time nonlinear program is solved with Ipopt (Wächter and Biegler, 2006) using the linear solver HSL MA57 (HSL, 2013).

5 RESULTS

Solutions to the optimal control problems specified in Section 4, applied to the vehicle models in Section 3, are here presented. The optimal control problems derived from Equation 35 and 36 are studied separately. Two different path functions are considered, both described by clothoid shapes. The first is a single clothoid curve, having a minimum curve radius of 30 m. The second path consists of two consecutive clothoid curves forming an S-like shape, with minimum radii of 10 m.

5.1 *Constant Velocity*

Figure 3 and 4 show the optimal solutions obtained for the objective defined by Equation 35, where the vehicle is constrained to a constant velocity. The solutions represent the maximum vehicle velocity predicted by the different models.

For the clothoid shaped path in Figure 3, the most prominent differences in the variable trajectories occur in the beginning of the maneuver, around $s = 50$ m. This can be derived to the roll dynamics, since it is visible for the pendulum model and the double-track model. However, the predicted maximum velocity are still very similar for all models, differing by only 0.2% at most.

In Figure 3, solutions to the path composed by two successive clothoid curves are shown. Here, the maximum velocity found for the double-track model is significantly lower, and the variable trajectories are clearly differing, compared to the pendulum model and the point-mass model. This is a consequence of the tire forces, in the double-track model, being unable to excite the yaw dynamics quickly enough. This is also verified by the later load-transfer $\Delta F_{z,r}$ not being a limiting factor at any point in the maneuver. This means the double-track model is not limited by rollover, but rather road friction and vehicle inertia properties.

5.2 *Braking*

Figure 5 presents the solutions obtained with the cost function defined by Equation 36, for the double-track model and the point-mass model. The path is the same clothoid-shaped curve as in Figure 3. The vehicle is given an excessive initial velocity of $v_0 = 72$ km/h (compare with the maximum velocities presented in Figure 3). The minimum-time formulation implies the vehicle

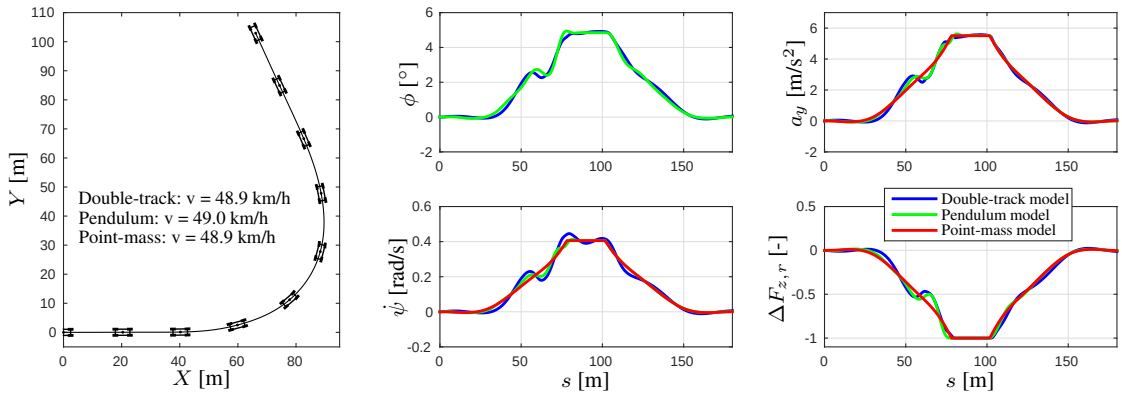

Figure 3. Optimal solution for the double-track model, the pendulum model, and the point-mass model driving through a clothoid shaped curve, with minimum radius of 30 m. Variables shown are the roll angle ϕ, lateral acceleration a_y, yaw rate $\dot{\psi}$, and rear-axle lateral load-transfer $\Delta F_{z,r}$. The leftmost plot display the global vehicle position (X, Y) and the obtained maximum velocities.

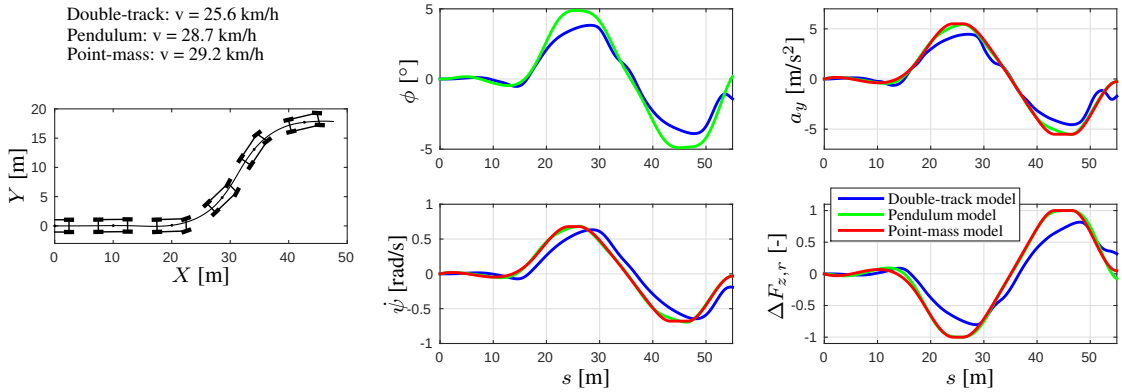

Figure 4. Optimal solution for the vehicle models driving through two successive clothoid curves with minimum radii of 10 m.

will maintain the highest possible velocity and initiate deceleration as late as possible, using minimal brake actuation.

The double-track model is seen to activate braking later, by barely 4 m, and with a larger deceleration magnitude. This is particularly evident for the longitudinal acceleration a_x shown in Figure 5. Nevertheless, the velocity profiles for both models align well throughout the braking phase. Following the braking phase, the double-track model is seen to scrub off additional velocity. This is a result of the front lateral tire-forces contributing to forces in the longitudinal direction, due to a non-zero steering angle δ.

Assume the above results are satisfying enough to motivate the use of a rollover-prevention controller based on the point-mass model. The controller would be able to compute the velocity profile, and subsequently the needed braking effort. However, the scheme for distributing the braking effort between the wheels is not evident. Therefore, a more straightforward strategy for braking-force distribution is here compared to the optimal distribution.

In the optimal braking distribution employed by the double-track model in Figure 5, the braking effort on each wheel is chosen individually. This strategy will here be referred to as *Individual braking*. The alternative braking strategy, which is denoted *F_z-coupled braking*, distributes the braking torque T proportionally to the vertical tire force F_z, according to

$$\frac{T_1}{F_{z,1}} = \frac{T_2}{F_{z,2}} = \frac{T_3}{F_{z,3}} = \frac{T_4}{F_{z,4}}.$$

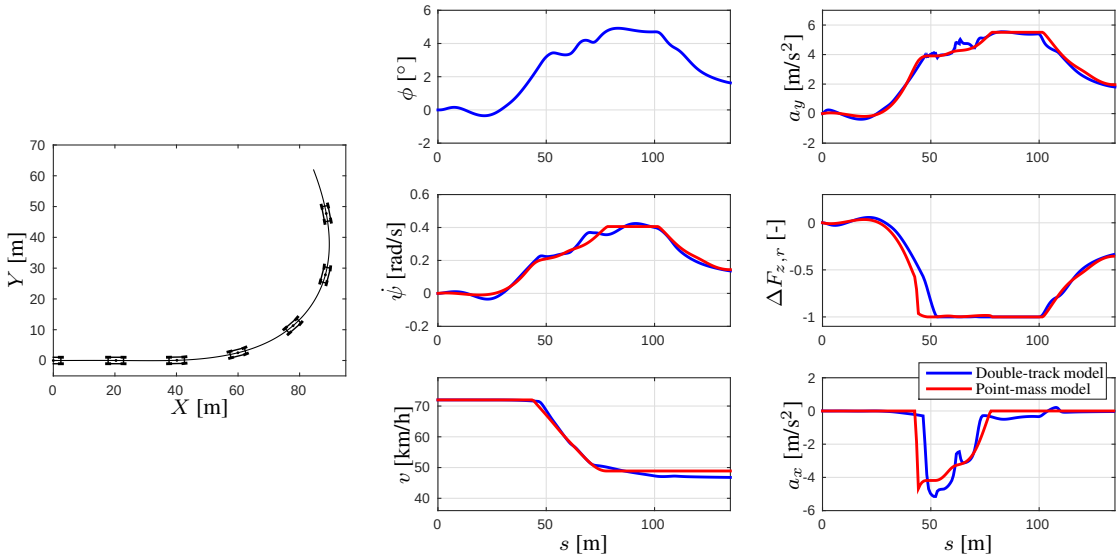

Figure 5. Time-optimal solutions for the double-track model and the point-mass model, driving through the clothoid-shaped path. The vehicle is here allowed to brake, but not accelerate.

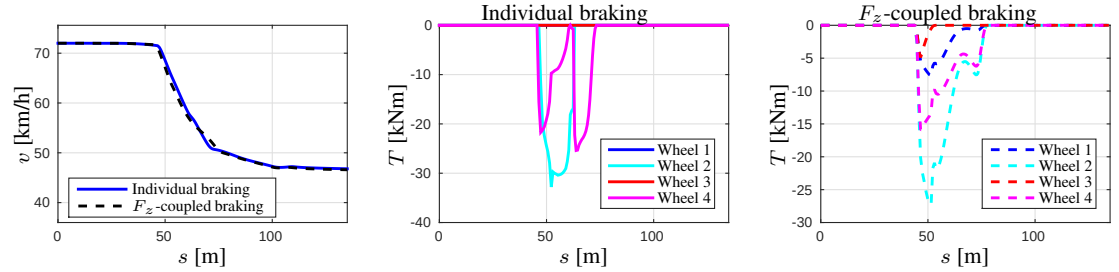

Figure 6. Velocity profile and wheel braking torque for the two different braking strategies, obtained for the time-optimal maneuver.

Figure 6 shows the velocity profile and wheel braking torque obtained for these two braking strategies when employed in the same time-optimal problem as in Figure 5. The *F_z-coupled braking* initiates braking earlier here, however, only by 1.6 m.

6 CONCLUSIONS

Three different vehicle models of different complexity were employed in optimal control problems, aimed at evaluating the rollover-prediction and rollover-prevention abilities. Optimization problems were solved where the maximum velocity for a given path was obtained, granted rollover was avoided. Subsequently, a second optimal control problem was formulated to address the situation of overspeeding into a road curve.

For paths with larger road curve radii, the simple models have the same ability to predict rollover in terms of maximum speed for a given path, as the high-fidelity vehicle model. For narrower turns, the complex and simple models starts to deviate. However, this is rather coupled to the yaw dynamics, road friction, and yaw inertia, than the rollover characteristics.

The point-mass model also shows promising results for velocity-control based rollover prevention. Compared to the much more complex vehicle model, the resulting velocity profile and braking actuation are remarkably similar. With the simplified model, information about the optimal braking distribution is lost. However, with a straightforward braking distribution, based on the vertical tire forces, only a minor loss in performance is seen, when compared to the optimal

braking distribution. This indicates the brake-force distribution is not essential for this application, as long as the total braking effort is maintained.

REFERENCES

Andersson, J. 2013. *A General-Purpose Software Framework for Dynamic Optimization*. PhD thesis, Arenberg Doctoral School, KU Leuven, Department of Electrical Engineering (ESAT/SCD) and Optimization in Engineering Center, Kasteelpark Arenberg 10, 3001-Heverlee, Belgium.

Cossalter, V., Lio, M. D., Lot, R., and Fabbri, L. 1999. A general method for the evaluation of vehicle manoeuvrability with special emphasis on motorcycles. *Vehicle System Dynamics*, 31(2):113–135.

HSL 2013. *A collection of Fortran codes for large scale scientific computation, http://www.hsl.rl.ac.uk/*.

Limebeer, D. and Rao, A. 2015. Faster, higher, and greener: Vehicular optimal control. *Control Systems, IEEE*, 35(2):36–56.

Liu, P., Rakheja, S., and Ahmed, A. K. W. 1997. Detection of dynamic roll instability of heavy vehicles for open-loop rollover control. *SAE Technical Paper: 973263*.

Pacejka, H. B. 2006. *Tyre and Vehicle Dynamics*. Butterworth-Heinemann, Oxford, United Kingdom, second edition.

Wächter, A. and Biegler, L. T. 2006. On the implementation of an interior-point filter line-search algorithm for large-scale nonlinear programming. *Mathematical Programming*, 106(1):25–57.

Winkler, C. B., Blower, D. F., Ervin, R. D., and Chalasani, R. M. 2000. *Rollover of heavy commercial vehicles*. Society of Automotive Engineers.